GEOPHYSICAL RESEARCH LETTERS, VOL. 38, L05602, doi:10.1029/2010GL046390, 2011

Source of microbaroms from tropical cyclone waves

Justin E. Stopa,[1] Kwok Fai Cheung,[1] Milton A. Garcés,[2] and David Fee[3]

Received 3 December 2010; revised 11 January 2011; accepted 18 January 2011; published 4 March 2011.

[1] Microbaroms are continuous infrasonic signals with a dominant frequency around 0.2 Hz produced by ocean surface waves. Monitoring stations around the globe routinely detect strong microbaroms in the lee of tropical cyclones. We utilize a parametric wind model and a spectral wave model to construct the tropical cyclone wave field and a theoretical acoustic source model to describe the intensity, spatial distribution, and dynamics of microbarom sources. This approach excludes ambient wave conditions and facilitates a parametric analysis to elucidate the source mechanism within the storm. A stationary tropical cyclone produces the strongest microbarom signals at the center, where the waves generated by the cyclonic winds converge. As the tropical cyclone moves forward, the converging wave field becomes less coherent and lags and expands behind the storm center. The models predict a direct relation between the storm forward speed and the location of maximum microbarom source intensity consistent with the infrasonic observations from Hurricane Felicia 2009 in the North Central Pacific. **Citation:** Stopa, J. E., K. F. Cheung, M. A. Garcés, and D. Fee (2011), Source of microbaroms from tropical cyclone waves, *Geophys. Res. Lett.*, *38*, L05602, doi:10.1029/2010GL046390.

1. Background

[2] Infrasound with frequencies below the audible threshold of 20 Hz comes from a variety of anthropogenic and natural sources. Of particular interest to studies of marine storms are the microseisms and microbaroms, which propagate respectively through the ground and the atmosphere with a dominant frequency around 0.2 Hz. *Benioff and Gutenberg* [1939] were among the first who related microseism generation to ocean waves. *Longuet-Higgins* [1950] derived the theoretical framework of microseism generation from nonlinear interactions of ocean waves with equal frequency and opposite directions. *Kedar et al.* [2008] computed the spatial distribution of microseisms over the North Atlantic from hindcast data based on the spectral wave model WaveWatch III (WW3) of *Tolman et al.* [2002] and related the source intensity and locations to seismometer measurements.

[3] Microbaroms measured at the International Monitoring System (IMS) infrasound arrays provide a wealth of information for research into their origin. *Willis et al.* [2004] and *Hetzer et al.* [2008] respectively identified strong microbarom signals in the wake of extratropical and tropical cyclones and inferred their measurements to interactions between storm and ambient waves from global WW3 data. More recently, Hurricane Felicia of 2009 generated strong microbaroms across the North Central Pacific and provides a good example to illustrate the source location. Figure 1 shows the best track from the NOAA National Hurricane Center and infrasound data taken at IMS Station IS59, Kailua Kona, Hawaii. The spectrogram covers the microbarom band of 0.1–05 Hz during the course of the storm. Post-processing of the data with the Progressive Multi-Channel Correlation method shows detection of coherent arrivals. The detections are binned into 3° every 15 minutes with the arrival azimuths relative to station IS59. The coherent signals show a greater azimuth than the best track indicating the generation of the infrasound behind the storm.

[4] The IMS stations have provided consistent measurements of microbarom signals in the wake of tropical cyclones. *Longuet-Higgins* [1950] postulated that the motion of a cyclone increases the effective area of nonlinear wave interactions behind the storm, but a quantitative description of the source mechanism from the wave field is less evident. The complex wave field, the interaction with the background sea state, and reflection from coastlines make it difficult to identify the microbarom source within a tropical cyclone from measurements or hindcast studies of actual events. We instead utilize WW3 to produce high-resolution wave fields from a parametric tropical cyclone in the open ocean. The acoustic model of *Waxler and Gilbert* [2006] determines the microbarom source region as it relates to the dynamics of tropical cyclones and the associated wave spectra in the absence of ambient wave activities. The parametric model allows a systematic examination and generalization of the microbarom source with respect to the storm parameters, which play an important role in the wave pattern. The measured data at IS59 from Hurricane Felicia allows examination of the model results based on idealized conditions.

2. Modeling of Tropical Cyclone Waves

[5] Tropical cyclones are intense storms with large gradients of wind speed and dynamically changing wind directions. The vortex of most tropical cyclones is clearly defined and can be represented by a parametric model with concentric circles of isotachs. *Phadke et al.* [2003] extended the modified Rankine vortex model with spirally inward wind flows and storm forward speed and along with *Cheung et al.* [2003] and *Tolman and Alves* [2005] showed the resulting parametric model produces an accurate description of tropical cyclone wind fields. This parametric model instead of a dynamic model provides a convenient tool to generate the input wind field from central pressure, radius of maximum winds, and forward speed for a sensitivity study.

[1]Department of Ocean and Resources Engineering, University of Hawaii at Manoa, Honolulu, Hawaii, USA.
[2]Infrasound Laboratory, Hawaii Institute of Geophysics and Planetology, University of Hawaii at Manoa, Honolulu, Hawaii, USA.
[3]Wilson Infrasound Observatories, Geophysical Institute, University of Alaska Fairbanks, Fairbanks, Alaska, USA.

0094-8276/11/2010GL046390

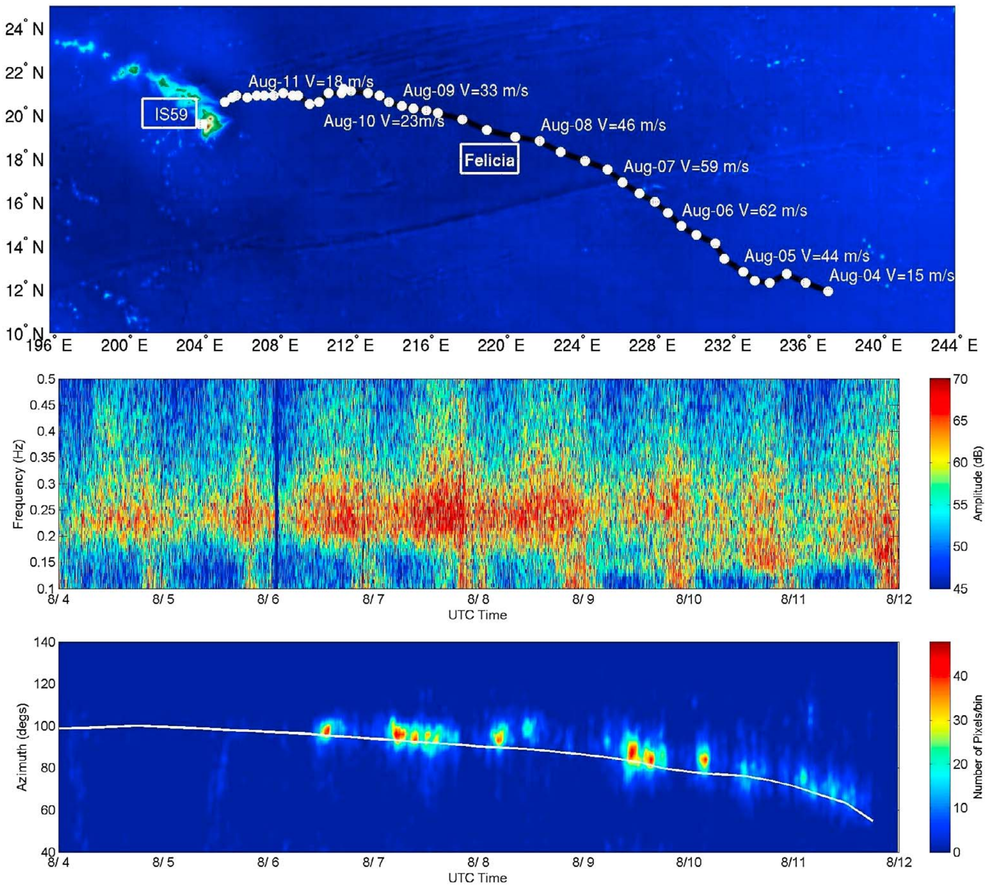

Figure 1. Best track of Hurricane Felicia of August 2009, amplitude of infrasound signals from IS59, and azimuths of coherent signals and storm location relative to station IS59 that demonstrate the microbarom source in the wake of the storm.

[6] WaveWatch III (WW3) (v3.14) is a third generation spectral wave model for wind wave generation and propagation [*Tolman et al.*, 2002]. When expressed in the Cartesian coordinates (x, y), the action balance equation, which describes evolution of the wave spectrum N in time t, is given by

$$\frac{\partial N}{\partial t} + \frac{\partial}{\partial x}\dot{x}N + \frac{\partial}{\partial y}\dot{y}N + \frac{\partial}{\partial k}\dot{k}N + \frac{\partial}{\partial \theta}\dot{\theta}N = \frac{S}{\sigma} \tag{1}$$

where k is wave number, θ is direction, $\sigma = 2\pi f$ is intrinsic angular frequency (f is the frequency), the over-dot represents the rate of change, and S denotes the source term for wind-wave interactions, quadruplet wave-wave interactions, dissipation through whitecapping, and dissipation due to bottom friction. The wave energy spectrum is obtained from $F(f, \theta) = N(k, \theta)/\sigma$ along with a Jacobian transform from k to f.

[7] *Waxler and Gilbert* [2006] developed a two-fluid model to describe radiation of atmospheric microbaroms by nonlinear interactions of ocean waves. The microbarom spectrum is computed from the wave spectrum as

$$D(f) = \left(\frac{4\rho_{air}^2 g^2 \pi^4 f^3}{c_{air}^2}\right)\left(\frac{9g^2}{4\pi^2 c_{air}^2 f^2} + \frac{c_{air}^2}{c_{water}^2}\right) \cdot \int_0^{2\pi} F\left(\frac{f}{2}, \theta\right) F\left(\frac{f}{2}, \theta + \pi\right) d\theta \tag{2}$$

where g is acceleration due to gravity, c_{air} and c_{water} are the speeds of sound in air and water, and ρ_{air} and ρ_{water} are the density of air and water. The integral in equation (2) was first proposed by *Hasselmann* [1963] to describe the wave directivity in a sea state. The acoustic power spectrum has double the frequency due to nonlinear interactions of opposing wave trains of equal frequency. The peak microbarom source energy can be expressed in decibels as

$$MB = 10\log_{10}\left(\max[D(f)]|A|/P_{ref}\right) \tag{3}$$

where $|A|$ is the WW3 computational cell area in m^2 and $P_{ref} = (20\ \mu\mathrm{Pa})^2/\mathrm{Hz}$ is the reference power spectral density for acoustic signals in air.

3. Results and Discussion

[8] Hurricane Felicia was category 4 at its peak. The NOAA Central Pacific Hurricane Center determined a maximum 1-minute sustained wind speed of 60 m/s and an average radius of maximum winds (Rmw) of 35 km from measurements taken by reconnaissance aircrafts. These parameters along with a zero forward speed provide the input to the parametric model for an initial assessment of the microbarom source mechanism. Figure 2 (left) shows the input wind field and the computed wave conditions as well as the microbaroms for the stationary tropical cyclone.

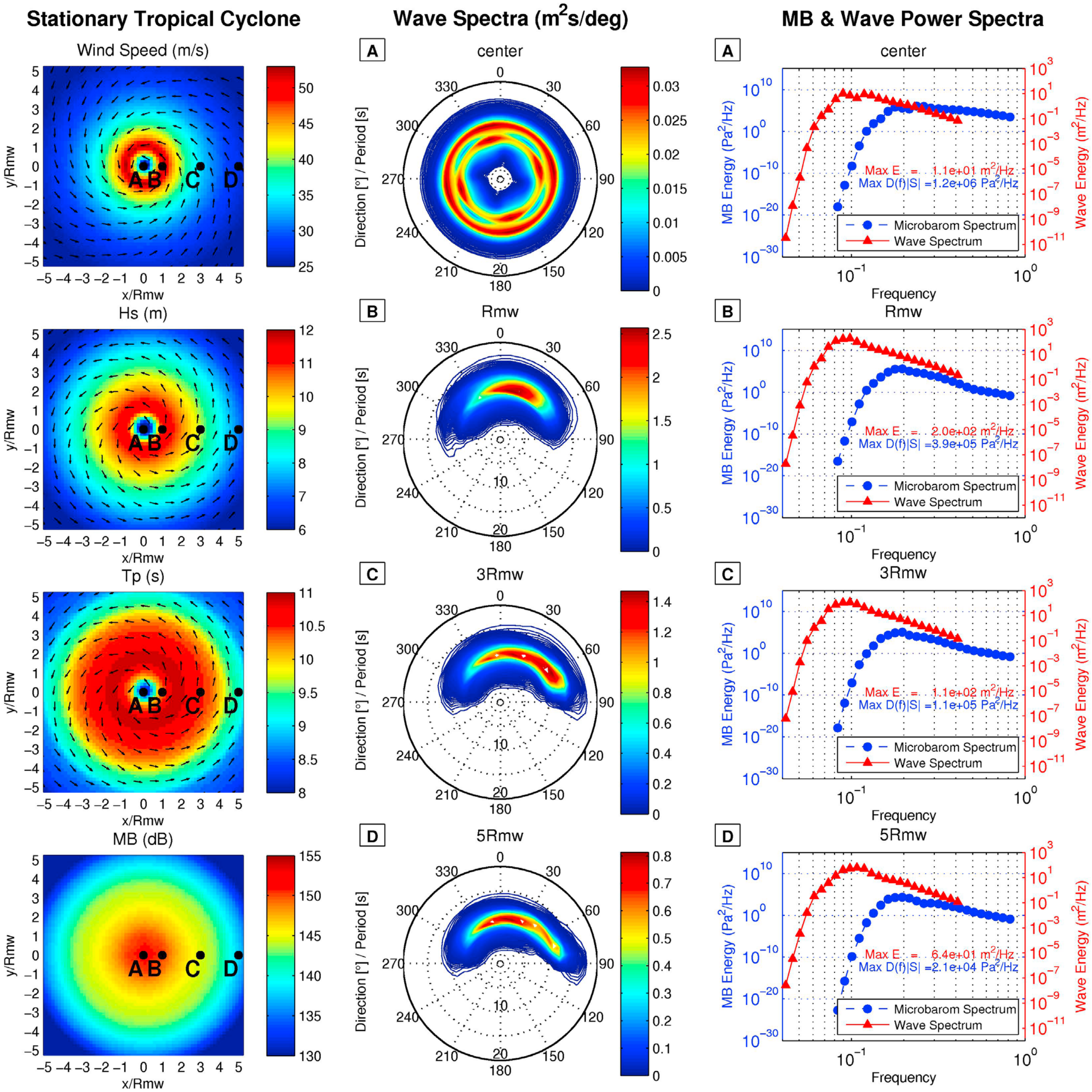

Figure 2. Data from parametric wind and spectral wave models to demonstrate the microbarom source mechanism in a stationary tropical cyclone. The points indicate the locations of the wave and microbarom spectra. The wave spectra cover a range of periods from 0 to 20 seconds.

The wind speed with a maximum of 54 m/s denotes the 8-minute average consistent with the WW3 source term. The axis-symmetric winds spiral toward the calm eye generating waves that propagate outward in a spiral pattern. The computed wave height and peak period have local minima of 3.4 m and 6 s at the center. The dominant wave energy propagates outward reaching a maximum significant wave height of 11.5 m and a peak period of 11 s just beyond the radius of maximum winds.

[9] Figure 2 (middle) shows the computed wave spectra at the storm center and at 1, 3, and 5 Rmw. The spectrum has a circular pattern at the storm center with waves of all directions over a large bandwidth of 2–14 s. The energy bands peaked at 6 and 10 s correspond to waves generated locally near the center and just outside the radius of maximum winds as inferred from the peak period plot. Away from the storm center, the wave direction covers a 200° window and is sufficient to produce microbaroms. The energy peak, however, becomes more spread-out beyond the radius of maximum winds. The spectra at 3 and 5 Rmw show three defined peaks around 340°, 15°, and 60° demonstrating the complexity of the wave field. Figure 2 (right) shows the corresponding wave and microbarom source spectra. The storm center has the largest acoustic energy due to the confluence of wave directions despite the local minimum of wave height. At the radius of maximum winds, there is an order of magnitude increase of wave energy from the center, but an order of magnitude decrease in acoustic energy due to

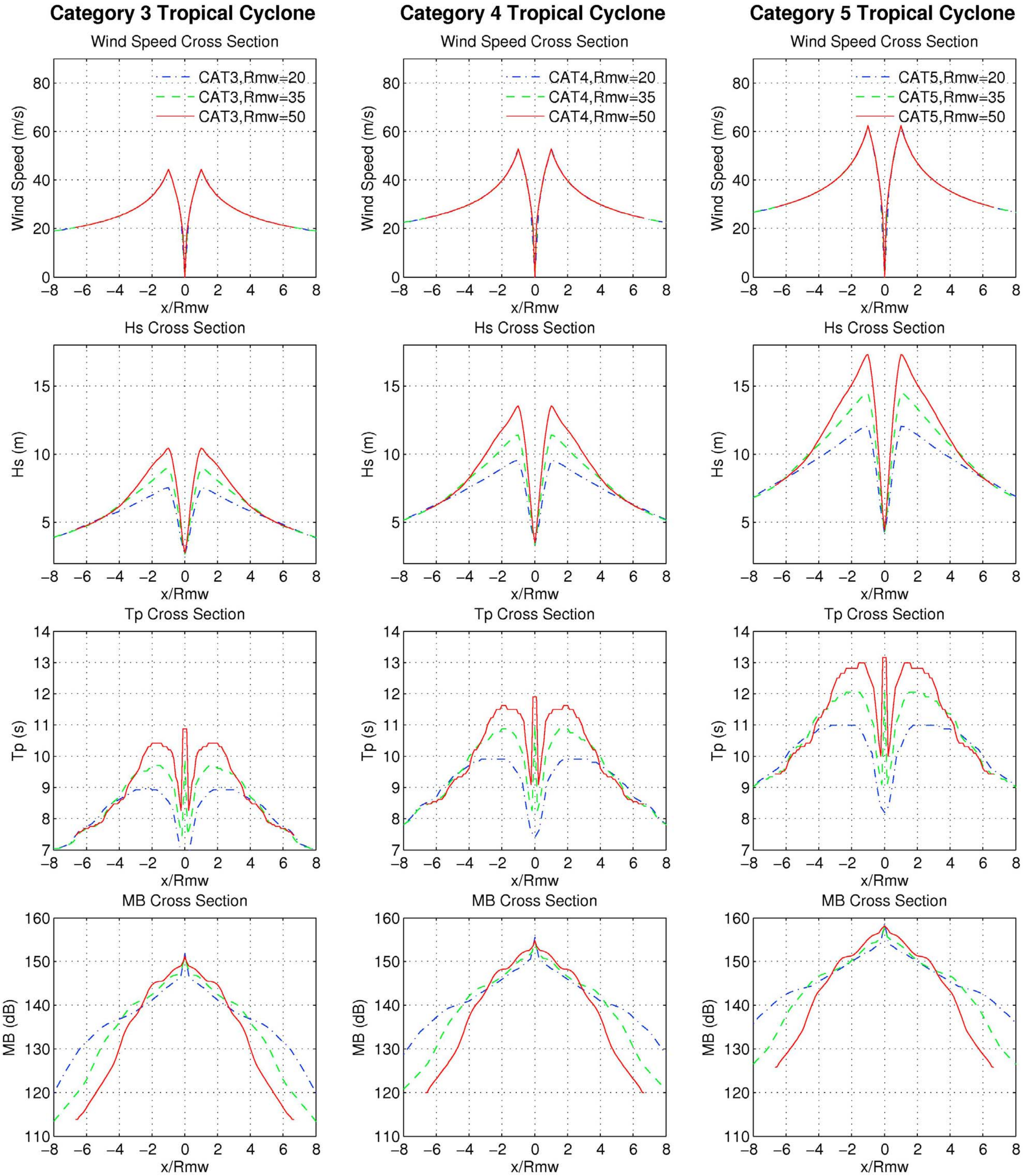

Figure 3. Wind speed, significant wave height, peak period, and microbarom energy across a stationary tropical cyclone as function of storm category and radius of maximum winds for a sensitivity analysis.

a less directional-spread wave field. The acoustic energy decreases gradually with the wave height beyond the radius of maximum winds while the directional spread of the wave spectrum remain constant.

[10] We also varied the intensity and size of the stationary tropical cyclone in a parametric analysis to examine their effect on the acoustic energy. Figure 3 shows the wind speed, significant wave height, peak period, and peak microbarom energy across category 3, 4 and 5 storms with Rmw of 20, 35, and 50 km. The results are plotted in radial distance normalized by Rmw. The wave height, peak period, and acoustic energy follow a linear trend with the storm intensity. For a given storm category, a larger storm results in larger wave heights and longer peak periods due to the

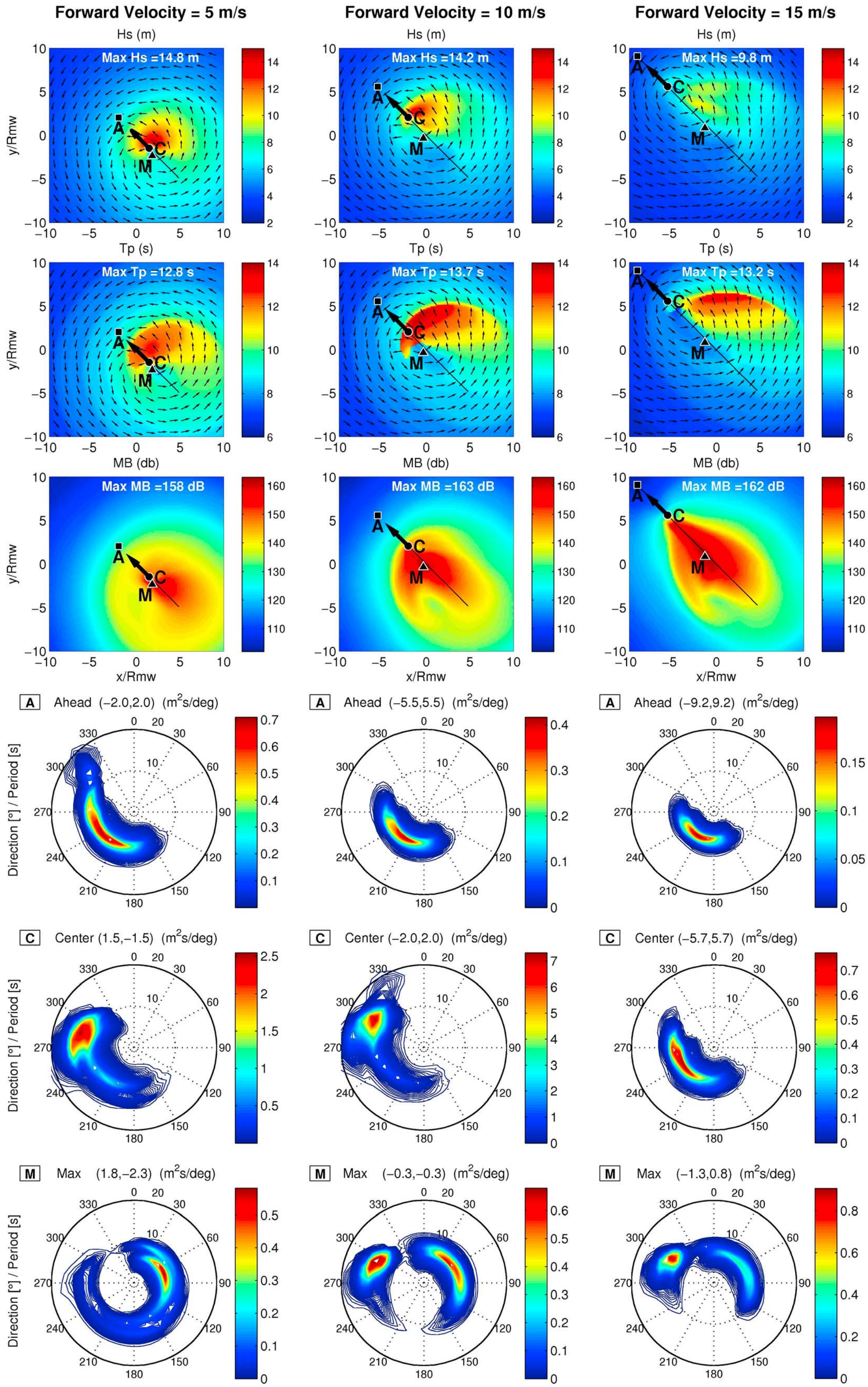

Figure 4. Significant wave height, peak period, microbarom energy, and wave spectra under a tropical cyclone as functions of forward speed. The spectra are at locations ahead of the storm (A), at the storm center (C), and at location of maximum acoustic energy (M) to demonstrate the microbarom source mechanism.

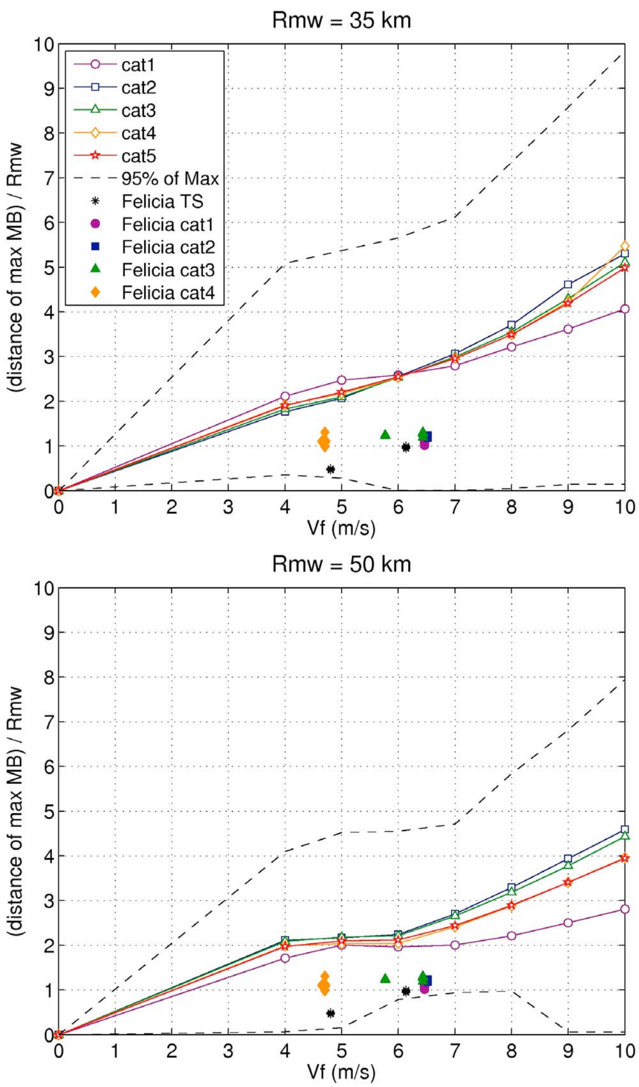

Figure 5. Location and extent of maximum microbarom energy versus forward speed to characterize the spatial distribution of the microbarom source behind the tropical cyclone.

increased fetch, while the microbarom energy at the storm center remains unaffected. In fact, its distributions in the peripheral show an inverse relation with the storm size. The waves in a larger storm have longer periods with less directional spread and are thus less efficient for microbarom generation. The peak microbarom energy does not appear to be a good measure of the storm size for a stationary storm in the absence of a background ocean wave field.

[11] The forward motion of tropical cyclones modifies the input wind conditions as well as the wave field. Figure 4 shows the variation of the wave conditions and microbaroms with storm forward speeds at 5, 10, and 15 m/s for a category 4 and 35-km radius tropical cyclone. The most dominant feature is the larger wave height to the right of the storm track where the forward motion adds to the wind speed and effective fetch. Maximum wave growth occurs for the forward speed of 10 m/s, which is slightly higher than the dominant group velocity of the resulting waves. At smaller forward speeds, the waves propagate ahead of the storm and disperse into swell. When the forward motion is faster than the dominant group velocity, the tropical cyclone outruns the wave field and shortens the effective duration for wave generation.

[12] The spatial extent of the microbarom energy increases behind the storm center consistent with the hypothesis of *Longuet-Higgins* [1950], but on the contrary, the peak energy level remains relatively uniform. Ahead of the storm, the wave spectrum at low forward speeds shows large directional and frequency spread. More waves lag behind at higher forward speeds and the spectrum becomes more unidirectional with less opposing waves for microbarom production. The spectrum at the storm center shows an energetic component at 13.5 s peak period for the forward speed of 10 m/s, but the production of microbaroms is mostly from the locally and previously generated waves below 10 s. The lagging of the waves as the forward speed increases also results in the shift of the maximum microbarom source behind the storm center. These waves generated previously at the front quadrants propagate against the locally generated waves in the wake of the tropical cyclones. The computed wave spectra show significant amounts of wave energy with opposite directions and same periods for microbarom production. The maximum microbarom energy level is located slightly to the left of the track due to opposing wave directions in the left front and rear quadrants.

[13] We included a typical range of forward speeds in the parametric analysis to examine the lagging of the microbarom signal behind the storm center. Figure 5 shows the lag of the maximum microbarom signal as a function of forward speed and storm category for Rmw = 35 and 50 km. At forward speeds below 4 m/s, the numerical results show multiple peaks in the rear quadrants due a combination of the chaotic sea state and the model resolution. The results at higher forward speeds show clear relationships between the location of the maximum microbarom signal with the radius of maximum winds and the forward speed. The lag of the maximum acoustic signal follows a linear trend with the forward speed, while the inverse relation between the energy level and storm size persists for moving tropical cyclones. The storm category also affects the location of the maximum signal but to an extent probably not distinguishable by instruments. The source region covers an extensive area behind the storm. The envelope of the 95% peak energy for all storm categories also expands with the forward speed. This high energy level extends beyond 10 Rmw behind the storm for a forward speed of 10 m/s.

[14] The results in Figures 4 and 5 show the peak microbarom signal occurs behind the storm center very close to the storm track. The measured azimuths of coherent acoustic signals and the best track allow estimation of the distance between the storm center and the peak microbarom signal for Hurricane Felicia to compare with the model results developed under idealized conditions. The inferred locations of the peak measured signal fall within the envelope of the 95% peak energy and follow a similar trend as the model data. Similar to the results from the parametric study, the storm category does not seem to have a strong relationship with the location of the peak acoustic signal. While the present study focuses on the microbarom source mechanism within a tropical cyclone, the interaction of the storm waves with the ambient wave field would likely expand the source

region of acoustic signals as inferred by *Willis et al.* [2004] and *Hetzer et al.* [2008].

4. Conclusions

[15] Tropical cyclone waves have produced microbaroms at infrasound stations around the globe. This study provides a quantitative description and verification of the source region within the storm through modeling of the wave field and the microbarom generation mechanism without interference from ambient conditions. A parametric study shows a stationary tropical cyclone generates the strongest microbarom signals at the center, where the waves generated by the cyclonic winds converge. The maximum acoustic energy shows a linear trend with the tropical cyclone category, but is relatively independent of the radius of maximum winds. The microbarom source region tapers off more rapidly for storms with large radii due to the more unidirectional waves as the fetch increases. This suggests the storm category, probably not the size, may to be reliably inferred from measured acoustic data.

[16] The forward speed of a tropical cyclone strongly influences the spatial distribution of microbarom sources consistent with *Longuet-Higgins*' [1950] hypothesis; however the peak acoustic energy remains relatively constant. Even at a forward speed slightly higher than the dominant wave group velocity with the most efficient wave growth, the maximum acoustic energy is not drastically affected. The source region, expands and shifts to the wake of the tropical cyclone with increasing forward speed. In the absence of ambient waves, the maximum acoustic energy is always located in the rear left quadrant close to the track where previously and locally generated waves with similar frequency bands propagate in the opposite directions. The microbaroms cover a large region with high energy and the peak location shows a linear trend with the forward speed as supported by data from Hurricane Felicia of 2009. The findings of this study have the implications to utilize infrasound measurements to gather weather information in sparsely covered and remote regions [*Garces et al.*, 2010].

[17] **Acknowledgments.** This paper is funded in part the National Oceanic and Atmospheric Administration, grant 09-09-022, for the project "Remote Infrasonic Monitoring of Natural Hazards". The authors would like to thank the two reviewers for their comments and suggestions that have improved this paper. SOEST contribution 8067.

References

Benioff, H., and B. Gutenberg (1939), Waves and currents recorded by electromagnetic barographs, *Bull. Am. Meteorol. Soc.*, *20*, 421.

Cheung, K. F., et al. (2003), Modeling of storm-induced coastal flooding for emergency management, *Ocean Eng.*, *30*(11), 1353–1386, doi:10.1016/S0029-8018(02)00133-6.

Garces, M., M. Willis, and A. Le Pichon (2010), Infrasonic observations of open ocean swells in the Pacific: Deciphering the song of the sea, Chapter in Infrasound Monitoring for Atmospheric Studies, edited by A. Le Pichon, Springer, Netherlands, doi:10.1007/978-1-4020-9508-5_7, p. 235–248.

Hasselmann, K. (1963), A statistical analysis of the generation of microseisms, *Rev. Geophys.*, *1*, 177–210, doi:10.1029/RG001i002p00177.

Hetzer, C. H., R. Waxler, K. E. Gilbert, C. L. Talmadge, and H. E. Bass (2008), Infrasound from hurricanes: Dependence on the ambient ocean surface wave field, *Geophys. Res. Lett.*, *35*, L14609, doi:10.1029/2008GL034614.

Kedar, S., M. Longet-Higgins, F. Webb, N. Graham, R. Clayton, and C. Jones (2008), The origin of deep ocean microseisms in the North Atlantic Ocean, *Proc. R. Soc. A*, *464*(2091), 777–793, doi:10.1098/rspa.2007.0277.

Longuet-Higgins, M. S. (1950), A theory on the origin of microseisms, *Philos. Trans. R. Soc. London, Ser. A*, *243*(857), 1–35, doi:10.1098/rsta.1950.0012.

Phadke, A. C., C. D. Martino, K. F. Cheung, and S. H. Houston (2003), Modeling of tropical cyclone winds and waves for emergency management, *Ocean Eng.*, *30*(4), 553–578, doi:10.1016/S0029-8018(02)00033-1.

Tolman, H. L., and J. H. G. M. Alves (2005), Numerical modeling of waves generated by tropical cyclones using moving grids, *Ocean Modell.*, *9*(4), 305–323, doi:10.1016/j.ocemod.2004.09.003.

Tolman, H. L., B. Balasubramaniyan, L. D. Burroughs, D. V. Chalikov, Y. Y. Chao, H. S. Chen, and V. M. Gerald (2002), Development and implementation of wind-generated ocean surface wave models and NCEP, *Weather Forecast.*, *17*(2), 311–333, doi:10.1175/1520-0434(2002)017<0311:DAIOWG>2.0.CO;2.

Waxler, R., and K. E. Gilbert (2006), The radiation of atmospheric microbaroms by ocean waves, *J. Acoust. Soc. Am.*, *119*(5), 2651–2664, doi:10.1121/1.2191607.

Willis, M., M. Garcés, C. Hetzer, and S. Businger (2004), Infrasonic observations of open ocean swells in the Pacific: Deciphering the song of the sea, *Geophys. Res. Lett.*, *31*, L19303, doi:10.1029/2004GL020684.

K. F. Cheung and J. E. Stopa, Department of Ocean and Resources Engineering, University of Hawaii at Manoa, Honolulu, HI 96822, USA. (cheung@hawaii.edu)

D. Fee, Wilson Infrasound Observatories, Geophysical Institute, University of Alaska Fairbanks, Fairbanks, AL 99775, USA.

M. A. Garcés, Infrasound Laboratory, Hawaii Institute of Geophysics and Planetology, University of Hawaii at Manoa, Honolulu, HI 96822, USA.